CHAPTER 5

Correlation between change-over from Weak Anti Localization (WAL) to Weak Localization (WL) and coexistence of positive and negative magneto-resistance in S-doped $Bi_{1.5}Sb_{0.5}Te_{1.3}Se_{1.7}$

5.1 Introduction

The Discovery of topological insulators (TIs) provides a new playground for probing the physics behind quasi particles such as Majorana and Dirac fermions which have unusual dispersion relations[103], [121]. The 3D TIs has attracted much attention because of their linear dispersions, robust surfaces and spin momentum locking, which is beneficial in technological applications such as spintronics, potential applications in the quantum information process[122], [123]. For technical applications of TIs, it is required to handle the properties of Dirac carriers in the topological surface state (TSS) by keeping bulk insulating. In order to achieve a bulk insulating state, it is suitable to reduce the anti-site defects by changing the chemical characteristics. Bi_2Te_2Se (BTS) is a ternary tetradymite TI that is ordered in Te-Bi-Se-Bi-Te quintuple layer (QL) and has large bulk resistivity due to less defect formation[104], [124]–[127]. Similar to BTS, another quaternary tetradymite TI material $Bi_{2-x}Sb_xTe_{3-y}Se_y$ (BSTS), also exhibit a large resistivity[104], [106], [123]–[125], [127]. To get rid of bulk conduction and achieve the material as pure as possible, we have to choose a system like BSTS in which residual acceptors are compensated by the residual donors via composition tuning[128], [129].

The negative magneto-resistance (n-MR) in TIs is an interesting phenomenon and provide a path to explore the transport properties. n-MR has been observed under both perpendicular and parallel magnetic fields till now, such as in ultrathin Bi_2Se_3 film[130], in $Bi_2Se_{3-y}S_y$[131], in $(Bi_{1-x}Sb_x)Te_3$ thin film due to different mechanisms. Therefore, it is very interesting to understand the underlying mechanism behind the origin of n-MR in nonmagnetic TIs. BSTS is a promising candidate for TI series because a special combination of x and y gives some unique properties like good thermoelectric power at close to room

temperature[132], [133]. By changing the combination in an appropriate manner, we can control the position of the Dirac cone. In most of the previously reported papers, the study is based on the tuning of Dirac point of TI and TSS band by optimizing the chemical doping or adding the layer of another elements on the surface of TI[123], [134]. One special combination of BSTS series is $Bi_{1.5}Sb_{0.5}Te_{1.3}Se_{1.7}$ which is characterized as a good TI by quantum Hall effect (QHE) and scanning tunnelling spectroscopy (STS)[123], [124], [135]. Tunability of Dirac cone has been observed in some combination of BSTS.

In this letter, we have presented detailed transport properties and electronic structure study of the Sulphur (S) doped $Bi_{1.5}Sb_{0.5}Te_{1.3}Se_{1.7-y}S_y$ (y=5% and y=10% represented as BSTSS-5 and BSTSS-10, respectively). In Magneto-transport data, we have observed the coexistence of p-MR and n-MR at low temperatures, which we have discussed in detail below. The topological character of surface state (SS) bands can be seen in the ARPES.

5.2 Experimental

The BSTSS were synthesized by the modified Bridgeman method as has been reported elsewhere[60]. The prepared single crystals were characterized by X-ray diffraction (XRD) using a Rigaku (miniflex II) Powder diffractometer with Cu Kα radiation. The magnetic measurements were performed by using a Quantum Design SQUID magnetic properties measurement system (MPMS). Magneto-transport measurements were carried out by using the physical property measurement system (PPMS). Angle-resolved photoelectron spectroscopy (ARPES) measurement has been done with a μ-Laser ARPES system with a photon energy of 6.3 eV at 20K at HiSOR, Hiroshima University, Japan. The Laser spot size (on the sample) was less than 10 μm resulting in an intrinsic angular resolution of the setup of less than 0.05°. The overall instrumental energy resolution was estimated to be better than

5 meV. All the samples were cleaved in-situ at 30K along the c-axis in an ultrahigh vacuum better than 5×10^{-11}Torr[73]. A very clean mirror-like surface was obtained after cleaving. The samples are found to be stable for more than two days in the UHV chamber.

5.3 Results and discussion

XRD patterns of the samples are shown in figure 5.1(a). All the observed peaks are along (*00l*) planes only. All the diffracted peaks are indexed and confirmed the single-phase and belong to the rhombohedral ($R\bar{3}m$) space group. For further confirmation, we have performed a Laue pattern for BSTSS-5 and BSTSS-10 (shown in figure 5.1 (b) and (c), respectively). A Clear six-fold symmetry with a line revealed the good long-range ordering present in the samples confirming the single-crystalline nature of the samples.

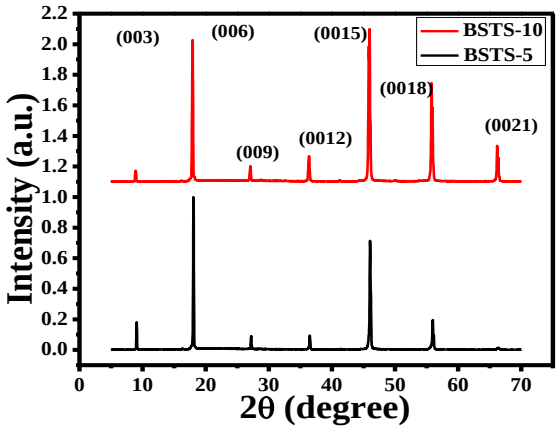

(a)

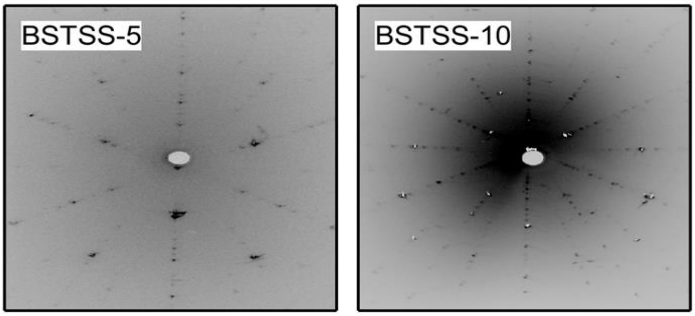

(b) **(c)**

Figure 5.1: (a) X-ray diffraction pattern of $Bi_{1.5}Sb_{0.5}Te_{1.3}Se_{1.7-y}S_y$ Topological insulators (b) Laue pattern of BSTSS-5 and (c) BSTSS-10.

Figure 5.2 shows the temperature dependence of resistivity for both samples. The insulating phase has been observed from the R-T curve, and it can be clearly seen that on increasing the sulphur content, resistivity value decreases. The resistivity behaviour of both the samples can be understood by different regimes, one is activated regime, which holds from 42K to 138K. The resistivity data can be fitted with the Arrhenius law in this temperature range:

$$\rho_{xx} = \exp(\Delta/K_B T) \quad (1)$$

Where K_B is the Boltzmann constant, Δ is the activation energy. We have fitted the Arrhenius equation on the experimental data with linear fitting to figure out the value of activation energy, displayed in figure 5.3 (a) and (c) for BSTSS-5 and BSTSS-10. The calculated value of Δ is very low 0.42 meV.

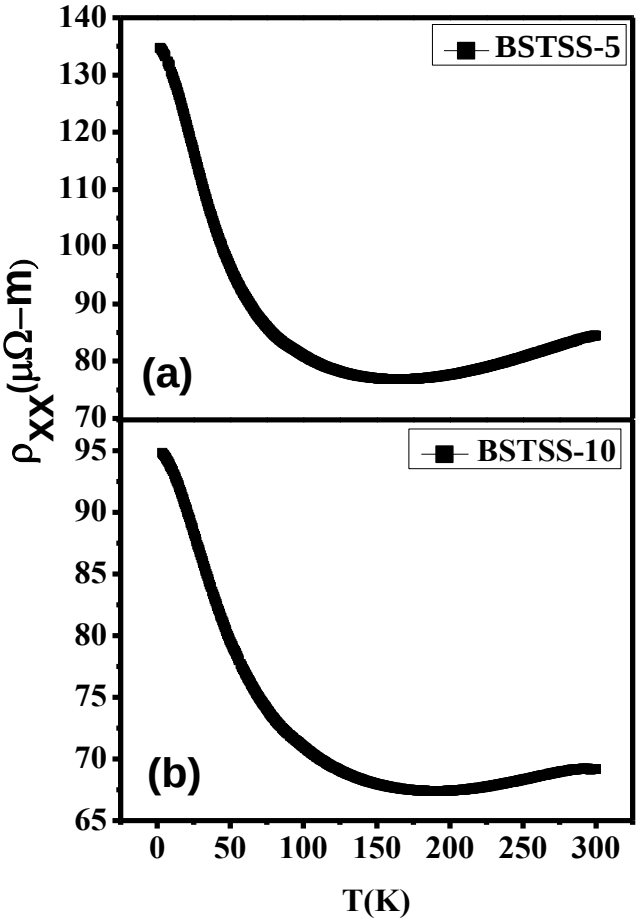

Figure 5.2: (a) and (b) Resistivity variation with temperature of BSTSS-5 and BSTSS-10.

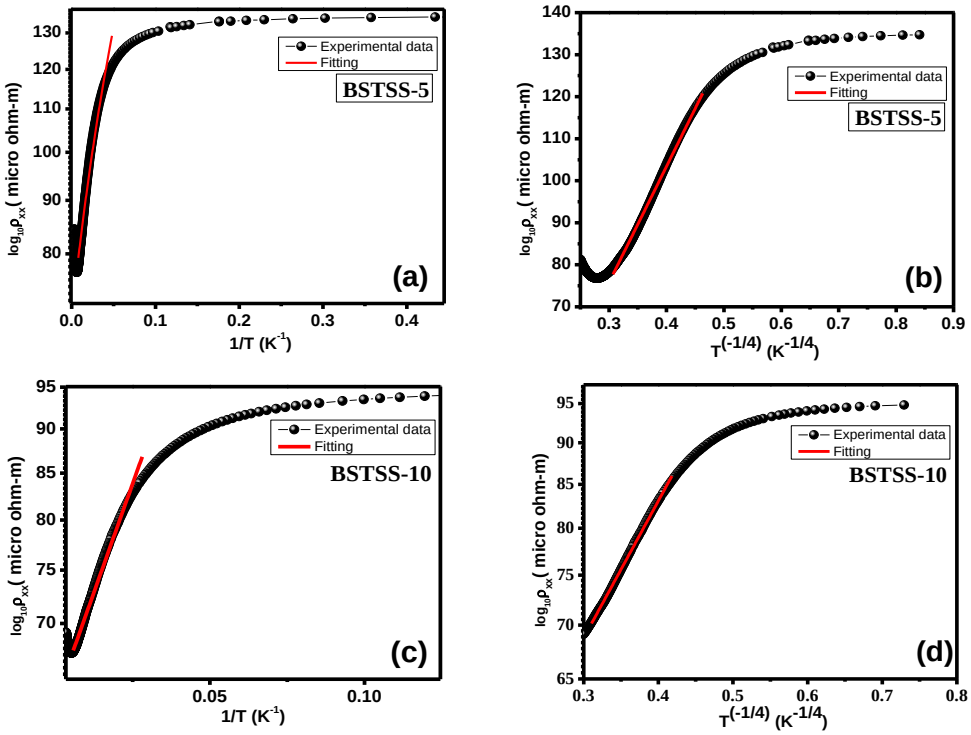

Figure 5.3: (a) and (c) Arrhenius Fitting of BSTS-5 and BSTS-10 (b) and (d) VRH fitting BSTS-5 and BSTS-10.

The insulating behaviour with temperature dependence can be understood by VRH (Variable range hooping) which is a hallmark of an insulator.

$$\rho_{xx} = \exp(T_0/T)^{-1/4} \quad (2)$$

The second one is the VRH behaviour which sustains from 35K to 126K, as shown in figure 5.3(b) and (d). However, this temperature range overlaps with the activated behaviour hence the distinction between both is ambiguous. We noticed a slight upturn at 300K; the decrement in carrier mobility or reduction in carrier concentration might be the reason of this upturn. In order to understand the mechanism for this kind of behaviour of resistivity, we have carried out the Hall measurement for both the samples (figure 5.4). The variation of Hall resistance with the magnetic field shows linear behaviour and almost independent of temperature. The linear and n-type nature of Hall data interpret that the transport is ruled by

single charge carriers (i.e., electron) and the temperature independency suggests that the carrier density is unaffected by temperature. With the help of Hall and resistivity data, we have calculated the carrier concentration and mobility by using the relation:

$$n=1/ R_{\circ}e, \ \& \ \mu=R_{\circ}/R_{xx} \tag{5.1}$$

Where $R_{\circ}$ is the Hall coefficient, e is the charge of electron and R_{xx} is the resistivity. We also calculated the value of surface carrier concentration n_s by by Shubnikov de Hass (SdH) oscillation calculation. The obtained parameters from Hall and SdH calculation are shown in the table 5.1.

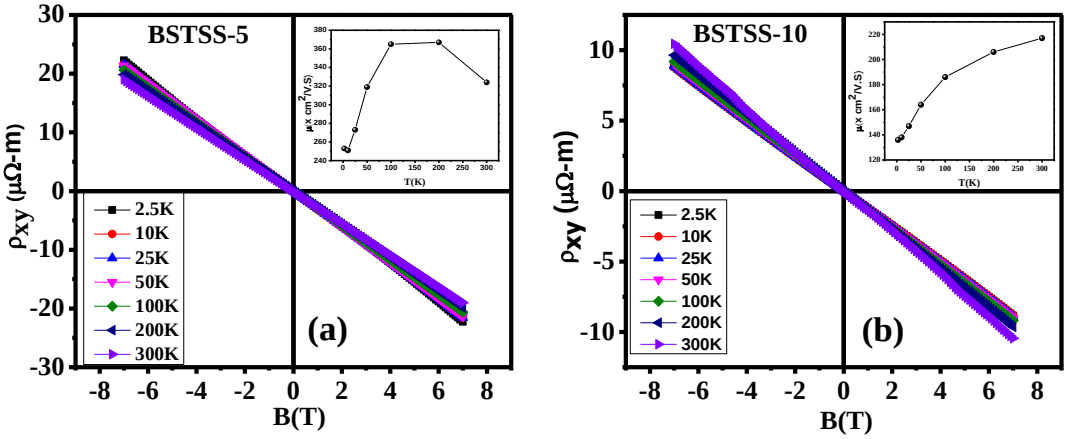

Figure 5.4: The variation of Hall resistivity as a function of applied magnetic fields of $Bi_{1.5}Sb_{0.5}Te_{1.3}Se_{1.7-y}S_y$ (a) BSTSS-5, (b) BSTSS-10 at different temperatures (mobility vs Temperature curve in inset).

A close inspection of the calculation brings out the following important results: i) the carrier concentration increases on increasing the S content and it is temperature independent. ii) In both the samples, the mobility is decreased on decreasing the temperature. The decrement in the Hall mobility ($\mu=e\,\tau\,/m$) insinuates that the scattering time is decreased and thus suggests that the S content induces the disorder. iii) Further from SdH and Hall calculation we have obtained Ioffe-Regel parameter [$K_fl=(3\pi n)^{2/3}(\hbar\mu/e)$] which decreases

with decreasing S content and it reaches close to 1 at low temperature (2K) in lower doped sample (BSTSS-5). This indicates the induced-disorder in both the compositions leads to localization of carriers supporting the upturn in ρ(T) for both the samples[136]. The value of Ioffe-Regel parameter is consistent with our experimental resistivity data, as for lower doping, resistivity shows more upturn than that of the higher doping. It suggests that S doping in BSTS leads to rise the disorder but further increment in S doping reduces the disorder.

Table 5.1: obtained parameters from Hall effect measurements, SdH calculation and Ioffe - Regel parameter.

Sample	**n_b (by hall calculation at 2K) (cm^{-3})**	**n_b (by SdH calculation at 2K) (cm^{-3})**	**n_s (by SdH calculation at 2K) (cm^{-2})**	**Mobility (by hall calculationat 2K) ($cm^2/V.S$)**	**Ioffe-Regel parameter (K_fl)**
BSTSS-5	1.83×10^{18}	4.15×10^{18}	1.97×10^{12}	136	1.107
BSTSS-10	4.74×10^{18}	3.04×10^{18}	1.60×10^{12}	253	3.951

Topological insulators have unique band structure due to which they show quantum phenomenon such as large linear magneto-resistance, Weak Localization(WL) effect and Weak antilocalization (WAL) effect[137]. To gain more insights of their transport properties, we have performed temperature and field dependent resistivity measurement. Figure 5.5 interprets the percentage magneto-resistance (MR%) for both the samples with the perpendicular magnetic field at different temperatures. The MR can be defined as:

$$MR = [R(H)-R(0)]/R(0) \times 100\% \quad (5.2)$$

Where, R(H) and R(0) are in-field and zero-field resistivity, respectively. We notice the temperature and field dependent competition between the positive magneto-resistance (p-MR) and negative magneto-resistance (n-MR) for both the samples. From figure 5.5 we can observe that at low temperature and low magnetic field (B), p-MR is pronounced and on increasing magnetic field (above 2.5T) the slope changes from positive to negative. Similar kind of behaviour has been observed in BSTSS-10 with lower value of MR%. In order to study the possible origin underlying this MR anomaly, we have measured the MR at different temperatures as shown in the figure 5.5 (a) and (b). The magnitude of PMR is increased about 4% on increasing magnetic field at 2T and it turns in n-MR (~4%) at 2K for BSTSS-5 on further increment in field and the same trend is followed by BSTSS-10. Besides, we have observed a sharp dip at low magnetic field and low temperature range. In figure 5.5 (a) and (b), the MR curves clearly show a sharp cusp around 0T at low temperature range as a confirmation of WAL effect [138]. The WAL feature has been observed in many TIs under perpendicular magnetic field [139]–[141]. On applying magnetic field in the perpendicular direction, we get the information about the magnetic transport of surface state of TIs as well as under parallel magnetic field configuration bulk state electron leads the transport [8], [142]. The presence of WAL suggests that the surface state is dominating in this field and temperature range. The quantum linear MR model of Abrikosov's associates the linear MR to the energy dispersion of the gapless SS of TIs[138], [143]–[145]. The WAL effect is also related with the strong spin momentum locking at the TSS and mainly associated to the π-berry phase of TSS [139].

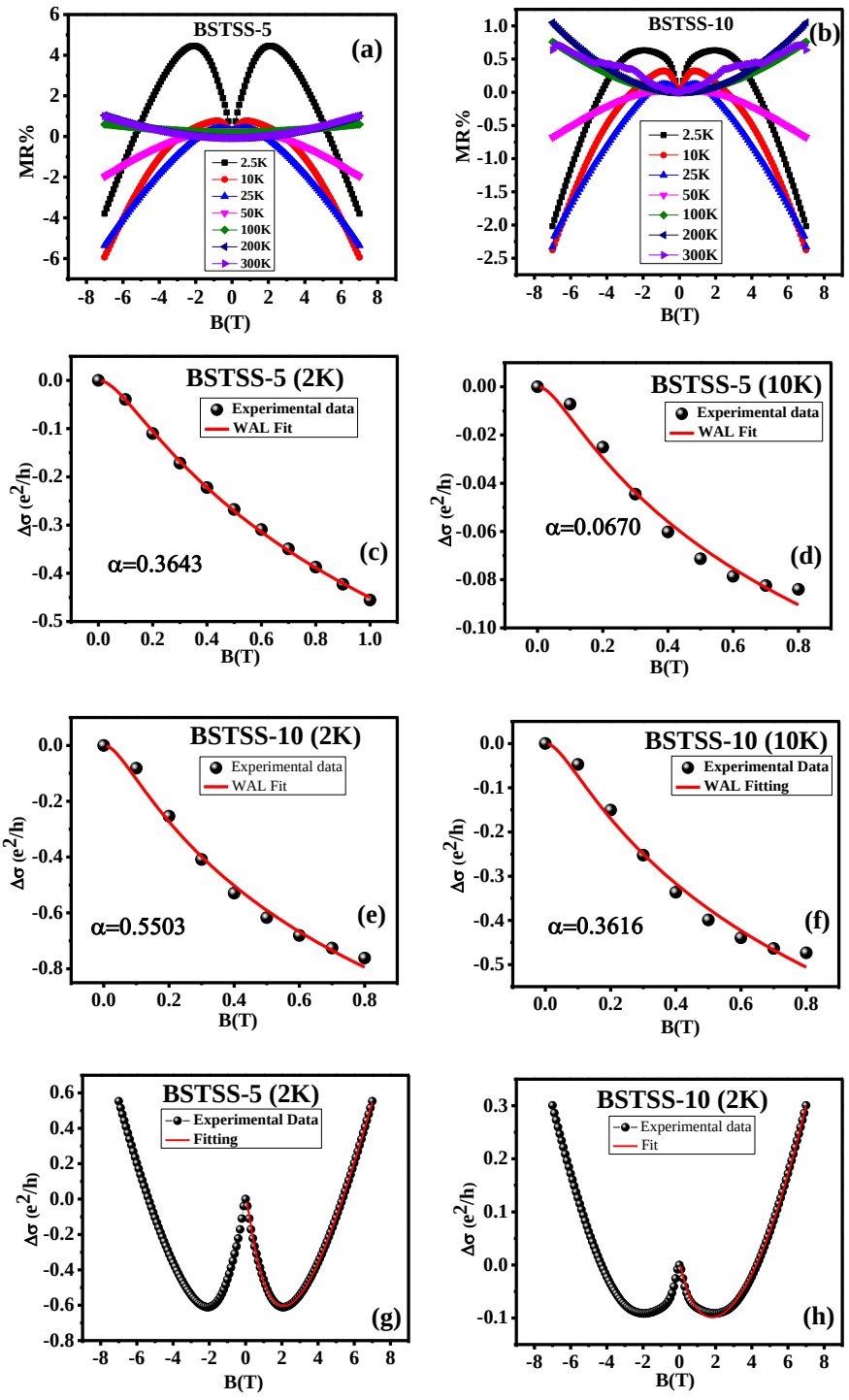

Figure 5.5: Magnetic field Variation of Magnetoresistance of $Bi_{1.5}Sb_{0.5}Te_{1.3}Se_{1.7-y}S_y$ (a) BSTSS-5 and (b) BSTSS-10 at different temperatures; WAL fitting (c) and (d) for BSTSS-5 and (e) and (f) BSTSS-10 at different temperatures; Fitting for n-MR correction (g) BSTSS-5 and (h) BSTSS-10.

Therefore, it is clear that the signature of WAL supports the presence of surface state (SS) in topological insulator which is also consistent with the ARPES results. At low temperature, the MR phenomenon can be divided into two regimes: regime-1 with p-MR at low field and low temperature (0 to 2T) and regime-2 with n-MR at high field (2 to 7T). It must be noted that, with increase in temperature, the magnitude of p-MR starts to decrease and n-MR is increased but further increase in temperature (T>50K) give rise to p-MR in the full range of magnetic field. The competition between p-MR and n-MR can be seen at low temperature range only (T<100K). Thus, the interplay between p-MR and n-MR is temperature and field dependent.

In order to inspect the observed interesting MR in detail, we study the reason behind such type of nature of MR. In figure 5.5, the linear p-MR with sharp cusp at low magnetic field, ascribed as due to WAL. The WAL phenomenon can be expressed by the Hikami-Larkin-Nagaoka (HLN) equation,

$$\Delta\sigma = \sigma(B) - \sigma(0) = A\left[\psi\left(\frac{1}{2}+\frac{h}{8\pi eBl_{\varphi}^{2}}\right) - ln\left(\frac{h}{8\pi eBl_{\varphi}^{2}}\right)\right] \quad (5.3)$$

Where l_{φ} represents phase coherence length, ψ is a digamma function and $A = \frac{\alpha e^2}{\pi h}$ represents to the number of conduction channel and α is the prefactor value. The value of α= -0.5 associated with π Berry phase of band. Figure 5.5 (c) and (d) shows magneto-conductivity (MC) curves $\Delta\sigma = \sigma(B) - \sigma(0)$ at low temperatures. We have fitted the data at the low temperature and low field with equation 5.3 to establish TSS and WAL effect. To calculate the value of conductance per conduction channel in 3D, we have to divide Δσ by Z (Z, number of conduction channel =t/2nm, where t is the thickness of sample). One 2D layer contributes 1(e^2/h) conductance and have 2QL which have thickness of 2nm[102]. The well fitted data of magneto conductance is shown in the figure 5.5 (c) and (d). We have determined

several parameters such as α=-0.3643 (2K) and -0.0670(10K) for BSTSS-5 and for BSTSS-10, α= -0.5503 (2K) and -0.3616 (10K), respectively. If the phase coherence length is larger than mean free path of electron, the MR shows sharp WAL cusp[146], [147]. Determined value of l_ϕ (2K) is 59nm (BSTSS-5) and 71.78nm (BSTSS-10), which is greater than the mean free path of BSTS system[81], [146]. All are in good agreement with the previously reported values[127], [146], [148]–[150].On increasing temperature, thermal scattering is increased and phase coherence length starts to decrease and WAL cusp is vanished [146], [150].

The switching of MR between p-MR and n-MR can be clearly seen in the figure 5.5 and the n-MR arises above 2T. The possible reasons of n-MR could be chiral anomaly, weak localization effect, Kondo effect, the formation of charge puddle, and many more. The n-MR is generally observed on applying parallel magnetic field. The most obvious reason is chiral anomaly which is observed on applying magnetic field parallel to the electric current but we measured the MR at perpendicular field. The n-MR due to Anderson localization exists when the Hall data shows the nonlinearity but our samples display linear Hall trend. Thus, we can rule out this possible reason. The other possible reason of this n-MR can be the Kondo effect due to presence of magnetic ordering in the system. In a metal, the scattering of conduction electron is due to magnetic impurity developing a characteristic change in resistivity at low temperature, known as Kondo effect. Therefore, resistivity shows upturn at low temperature range but our system has an insulating behaviour.

The switching of MR from p-MR to n-MR in our samples observed when magnetic field increases and it disappears as temperature increased. This is the prime feature of Weak localization(WL)[144], [151]. Both the samples show a prominent positive cusp in the range

-2T<B<2T and gives maximum peak at 2T and with further increase of magnetic field the peak value decreases similar to WL[136]. The crossover from WAL to WL is due to inflection from p-MR to n-MR and it will be elucidated in the detail below. The WL is the result of constructive interference of electron waves due to elastic scattering and gives negative quantum correction to resistance. In TIs, SOC is very strong in the bulk state which leads to WAL effect with positive quantum correction to the resistance at low magnetic field[8], [139]. Due to effect of quantum correction, MR is categorized into two-time scales; the dephasing time τ_Φ and spin flip time τ_{so}. If $\tau_\Phi >> \tau_{so}$, then spin orbit scattering is pronounced in which spins are flipped frequently and results into destructive quantum interference. In such case, WAL occurs and positive MR comes into the picture. In case of $\tau_\Phi << \tau_{so}$, spin orbit scattering is weak therefore it doesn't affect spin directions so much. As a result of it, n-MR occurs with high magnetic field as WL feature. In the intermediate state where $\tau_\Phi > \tau_{so}$, MR firsts increase to a maximum value and then starts to decrease, called a crossover from WAL to WL. Thus, the quantum interference behaviour of a system depends on the ratio of τ_Φ and τ_{so}[138].

In the TIs, the corresponding quantum correction to the bulk state conductivity is given by the equation.

$$\Delta\sigma = -\frac{e^2}{2\pi h}\left[\psi\left(\frac{1}{2}+\frac{B_\Phi}{B}\right) - ln\left(\frac{B_\Phi}{B}\right)\right] + \frac{3e^2}{2\pi h}\left[\psi\left(\frac{1}{2}+\frac{B_{so}}{B}\right) - ln\left(\frac{B_{so}}{B}\right)\right] \qquad (5.4)$$

This equation has two terms, which defined the competition between WAL and WL. The first term of the equation (5) defines the positive MR *i.e.* WAL effect (at low field) and the second term is responsible for the n-MR (WL effect) which is dominating on increasing magnetic field[8], [138]. Our experimental data for both the samples is very well fitted with equation 5.4 as depicts in figure 5.5 (g) and (h). From the fitting, we have obtained the

parameters l_{Φ} =44nm and l_{so}=20nm at 2K for BSTSS-5. As we know, $l_{\Phi} \propto (\tau_{\Phi})^{1/2}$ therefore $\tau_{\Phi} > \tau_{so}$, thus it falls into the intermediate state. As a result, the WAL arose at low field and when magnetic field is large enough, crossover into WL is taken place. Figure 5.5 (g) and (h) both owned to this case and crossover can be observed within 7T.

To probe the electronic band structure and topological surface state of the samples, we have performed ARPES measurement of the samples. Figure. 5 represent the high-resolution ARPES image plots on BSTSS-5 (a) and BSTSS-10 (b). The energy distribution curves (EDCs) taken at the $\bar{\Gamma}$-point (k_x=0) are shown in Figure.5.6(c), (d) for BSTSS-5 and BSTSS-10, respectively. The prominent linearly dispersing electronic energy Surface states (SS) bands are observed for both samples. The upper and lower part of the Dirac cone is touching each other at the Dirac point, which shows spin degeneracy of the Dirac bands. The position of Dirac point for BSTSS-5 is at 0.30eV and for BSTSS-10 is at 0.225eV. The EDC peaks at the Dirac point can be fitted by a single Lorentzian function suggesting the gapless TSS for BSTSS-5 and BSTSS-10 samples. The Dirac point for both the samples lies below the Fermi energy indicating that the carriers are electrons, which is consistent with Hall data and supports the n-type nature of the samples. The one intriguing thing is observed that on increasing doping percentage, Dirac Point lifts upwards. In the figure 5.6, it can be clearly seen that on increasing doping percentage, SS becomes more significant, supporting the reduced defects in BSTSS-10. This is also consistent with the WAL study. The value of obtained parameter (α) from HLN fitting for BSTSS-5 is 0.3643 and for BSTSS-10 is (0.5503) at 2K. A value close to 0.5 indicates that the SS is more pronounced than the lower one. The reduction in defects also can be seen in R-T and Hall data. The Hall data also supports the fact that it is a perfectly compensated system.

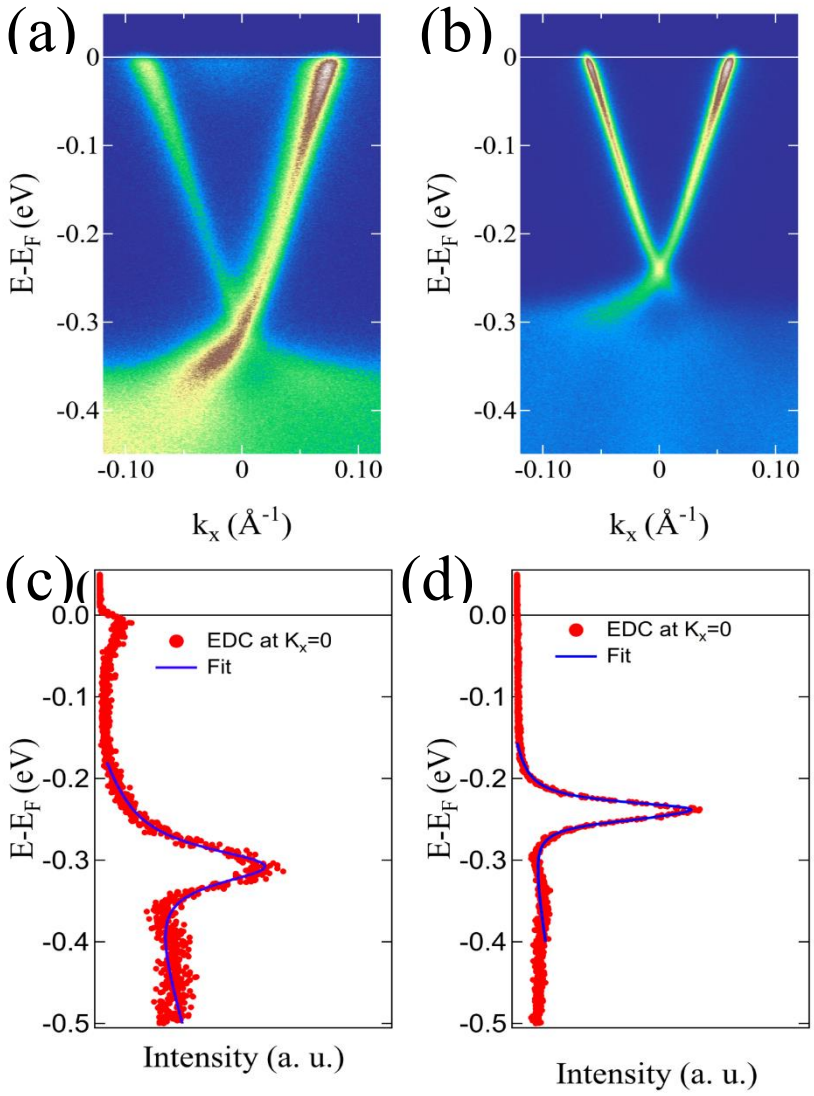

Figure 5.6: (a) and (b) ARPES spectra for BSTSS-5 and BSTSS-10 (c) and (d) Lorentzian Fit forBSTSS-5 and BSTSS-10 respectively.

5.4 Conclusion:

In summary, the impact of sulphur doping has been examined in S-doped BSTS system from magneto-transport, magnetization and ARPES measurements. Single phase and single crystalline nature of the samples were established from XRD and Laue's diffraction patterns. The insulating character has been confirmed from resistivity analysis which is a consequence

of the reduction in anti-site defects with sulphur doping. Furthermore, both p-MR and n-MR have been found on account of crossover from WAL to WL. Sharp linearly dispersing SS bands are perceived from the ARPES measurement, and it has been observed that on increasing doping concentration, Dirac Point lifts upwards. Overall, the role of sulphur doping is becoming very interesting because the doping percentage is playing a vital role in the transport phenomenon because, after S doping, the behaviour of Magnetoresistance is changed remarkably.